Biophysical Chemistry 254 (2019) 106266

Contents lists available at ScienceDirect

Biophysical Chemistry

journal homepage: www.elsevier.com/locate/biophyschem

# Molecular dynamics simulations of mechanical stress on oxidized membranes

Maria C. Oliveira[a], Maksudbek Yusupov[b], Annemie Bogaerts[b], Rodrigo M. Cordeiro[a,*]

[a] Centro de Ciências Naturais e Humanas, Universidade Federal do ABC, Avenida dos Estados 5001, CEP 09210-580 Santo André, SP, Brazil
[b] Research Group PLASMANT, Department of Chemistry, University of Antwerp, Universiteitsplein 1, B-2610 Antwerp, Belgium

## HIGHLIGHTS

- The membrane oxidation decreases the critical areal strain required for pore formation;
- Each oxidation product has a different effect over the membrane properties;
- Pore formation at domain boundaries was investigated to test whether interfaces are leaky;
- Due to large statistical variance and sensitivity to simulation conditions, results were inconclusive.

## GRAPHICAL ABSTRACT

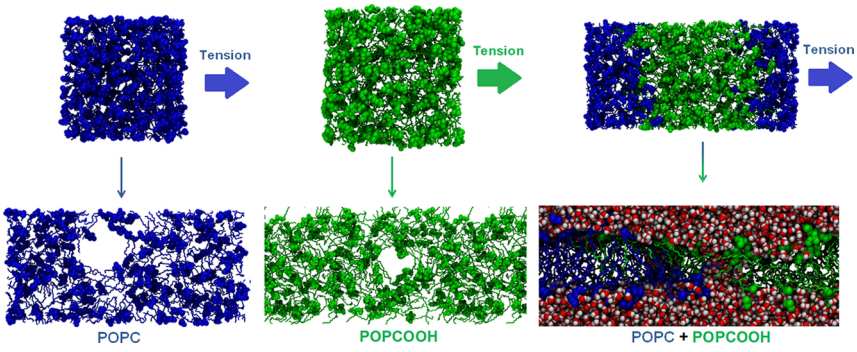


## ARTICLE INFO

*Keywords:*
Lipid oxidation
Membrane rupture
Pore formation
Domain interfaces

## ABSTRACT

Biomembranes are under constant attack of free radicals that may lead to lipid oxidation in conditions of oxidative stress. The products generated during lipid oxidation are responsible for structural and dynamical changes which may jeopardize the membrane function. For instance, the local rearrangements of oxidized lipid molecules may induce membrane rupture. In this study, we investigated the effects of mechanical stress on oxidized phospholipid bilayers (PLBs). Model bilayers were stretched until pore formation (or poration) using non-equilibrium molecular dynamics simulations. We studied single-component homogeneous membranes composed of lipid oxidation products, as well as two-component heterogeneous membranes with coexisting native and oxidized domains. In homogeneous membranes, the oxidation products with —OH and —OOH groups reduced the areal strain required for pore formation, whereas the oxidation product with =O group behaved similarly to the native membrane. In heterogeneous membranes composed of oxidized and non-oxidized domains, we tested the hypothesis according to which poration may be facilitated at the domain interface region. However, results were inconclusive due to their large statistical variance and sensitivity to simulation setup parameters. We pointed out important technical issues that need to be considered in future simulations of mechanically-induced poration of heterogeneous membranes. This research is of interest for photodynamic therapy and plasma medicine, because ruptured and intact plasma membranes are experimentally considered hallmarks of necrotic and apoptotic cell death.

* Corresponding author.
*E-mail address:* rodrigo.cordeiro@ufabc.edu.br (R.M. Cordeiro).

https://doi.org/10.1016/j.bpc.2019.106266
Received 25 April 2019; Received in revised form 9 September 2019; Accepted 12 September 2019
Available online 13 September 2019

## 1. Introduction

The major structural lipids in eukaryotic membranes are the phospholipids. They have a nearly cylindrical molecular geometry composed of saturated and *cis*-unsaturated fatty acyl chains, which render them fluid at room temperature [1]. These fatty acid chains of phospholipids can become oxidized through specific enzymatic pathways or reactions with free radicals, namely *reactive oxygen and nitrogen species* (RONS) in general.

The oxidative attack on fatty acid chains by free radicals may lead to oxidative stress situations, generating relatively stable and persistent reaction intermediates, and products bearing functional groups such as hydroperoxide, hydroxyl and truncated acyl chains, such as aldehyde and carboxylic groups [2,3]. These oxidized products affect the microscopic and macroscopic properties of the membrane, inducing structural changes related to the area per lipid [4], lipid order [5], bilayer thickness and bilayer hydration profile [6].

In addition, the structural and conformational changes in the membrane caused by lipid oxidation might induce pore formation [7]. There are several experimental studies, where cold atmospheric plasma (CAP), i.e., an ionized gas used for several medical applications, as it is a source of RONS, was applied to study lipid oxidation and its effects on the structural and chemical modifications and the transport of ROS across the membranes [8–13]. It was reported that CAP treatment of phospholipid vesicles results in an increased fluidity of the phospholipid bilayers (PLBs) [9] as well as chemical modifications on the phospholipids [10]. Moreover, it can cause an ingress of ROS into the vesicles, thereby having no damage in the membrane integrity [11]. The permeation of OH radicals across phospholipid vesicles and their subsequent interaction with intramembrane molecules was reported by Ki and co-workers [12], whereas the formation of pores was observed in artificial planar lipid bilayers [13].

Computer simulations applied to oxidized PLBs also revealed similar results [14–17]. It was demonstrated that oxidation of the phospholipids leads to an overall increase in the membrane permeability [14,15], pore creation [16,17] and bilayer disintegration [7], as well as a change in the lipid mobility in the PLB [4]. Furthermore, pore formation can also be induced by electric fields generated e.g., by CAP. Indeed, some CAP sources can create strong electric fields which are high enough to induce pore formation in membranes [18–20]. A synergistic effect of RONS and electric field was reported, i.e., lipid oxidation can facilitate pore formation induced by electric fields [17]. Similar conclusions were made in an earlier study [21], where it was shown by the combination of computer simulations and experiments that oxidation of phospholipids enhances the susceptibility of the membrane to electropermeabilization.

The improvement of the cell membrane permeability was also observed by Kaneko et al. using a cell-solution electrode CAP [22]. The authors concluded that the increase of the membrane permeability is due to the electric field and the density of the short-lived ROS reaching the cells in the solution. Using phospholipid vesicles, Tai et al. also observed that OH radicals result in a significantly higher lateral fluidity of the membranes, whereas hydrogen peroxide has little effect [23]. In general, we can conclude that lipid oxidation might affect the bilayer fluidity and lipid disorder, thereby altering the membrane permeability.

Experiments [24] and theoretical works [25] have shown that lipid aldehydes may disrupt chemical gradients when incorporated to membrane mimetic systems, but the mechanism by which they induce membrane permeabilization needs to be better understood. On the other hand, membranes composed entirely of lipid hydroperoxides are able to maintain the membrane integrity [6,26].

Injuries to the membrane can affect the form, function, and survival of the cell. Oxidized membrane phospholipids are involved in various pathological conditions including cancer [27], atherosclerosis [28], Alzheimer's disease [29], infection and inflammation [30]. Moreover, lipid oxidation may induce liquid-ordered/liquid-disordered phase separation in membranes, forming cholesterol and sphingolipid-enriched raft domains, which might play fundamental active roles on cellular homeostasis and signaling [31,32]. Therefore, oxidatively-induced phase separation might have serious consequences for cell membranes that are subject to oxidative stress.

Recently, theoretical works have demonstrated that the interfaces between phase-separated domains are regions where pore formation is facilitated [33]. Tsubone and co-workers proposed that the lipid hydroperoxide, a cylindrical oxidized lipid, is a promoter of liquid-ordered/liquid-disordered phase separation, whereas lipid carboxylic acid, a conical oxidized lipid, does not cause phase separation, but influences directly the bilayer deformation and membrane leakage [34].

It is challenging to understand the lipid phase behavior of biomembranes due to the large size of the lipidome and the presence of large amounts of membrane proteins [35]. Moreover, while coexisting phases can be easily observed by fluorescence microscopy of model membranes, domains are harder to find in biomembranes of living cells. The domains might exist but could be too small to be observed, being smaller than the wavelength of light ($< 300$ nm) [36,37]. Thus, the molecular structure and the membrane properties at domain interfaces still need to be elucidated.

To understand membrane poration, biomechanical experiments based on biomembrane force probes have been conducted. Micropipette aspiration experiments are performed under static or at least quasi-static stress on giant bilayer vesicles [38]. The membrane rupture occurs when the stress or strain of the membranes exceeds critical values, depending on the lipid composition and concentration of cholesterol molecules [39].

Pore formation on lipid bilayers is an extremely rapid event, triggered by a molecular-scale rearrangement of membrane structure. Hence, it is also difficult to capture details of pore formation through experimental methods. Besides that, the pore is unstable: depending on the intensity of the applied stresses on the bilayer and the pore radius, the pore can spontaneously close or continue to grow indefinitely, leading to membrane rupture [40,41]. Moreover, the presence of ions may influence the critical stress. In particular, adsorption of sodium ions to the membrane results in a higher critical stress due to a stiffened membrane. Consequently, the mechanical stress needs to be increased in order to yield stable pores [42].

The mechanisms by which lipid oxidation affects membrane properties need to be better understood. *Molecular dynamics* (MD) simulations have been proven as a powerful tool to get information concerning structural and dynamic properties of membranes. Based on that, in this research we performed non-equilibrium MD simulations at atomistic level using two types of model membranes, i.e., the single-component homogeneous PLBs and a two-component heterogeneous PLB. We studied four different model membranes in the case of the single-component homogeneous PLBs, which either contained native (one system) or oxidized lipids (three systems). In the case of the heterogeneous system, we investigated a membrane with coexisting native and oxidized phospholipid domains. Our aim was to determine how lipid oxidation affects the permeability of biomembranes.

## 2. Methods

### 2.1. Description of the model membranes

We performed MD simulations to study the mechanical instability on PLB models due to lipid oxidation, in order to access atomistic information about how easy it is to form a pore. POPC (1-palmitoyl-2-oleoyl-*sn*-glycero-3-phosphocholine) is a well-studied phospholipid model that is a major component of eukaryotic biomembranes [43,44]. The structure comprises a *sn*-glycerol-3-phosphate esterified at the C1 and C2 positions to chains, and a phosphate and choline group, described by stereospecific numbering (*sn*) which refers to the C1 and C2 of the glycerol as *sn*-1 and *sn*-2 position, respectively. POPC can be oxidized at the double bond of its unsaturated (*sn*-2) fatty acid chain.

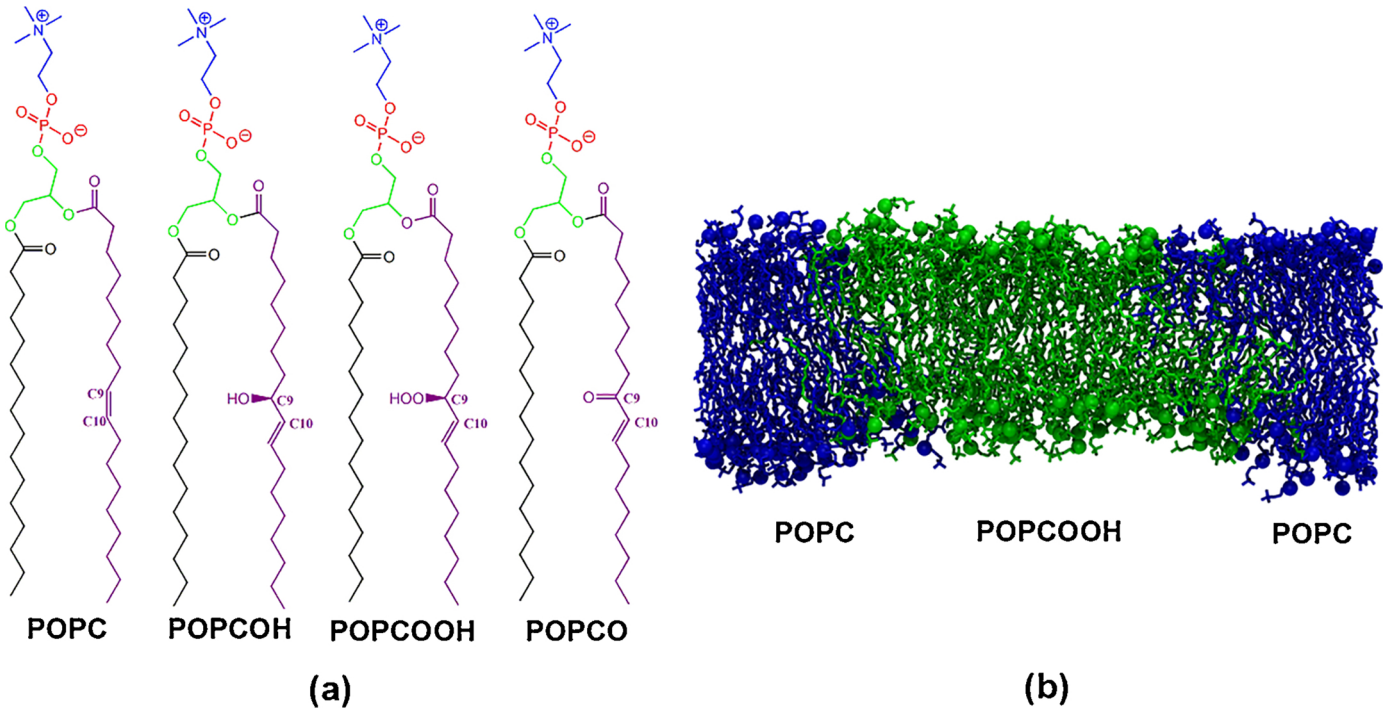


**Fig. 1.** (a) Structure of the POPC molecule and its oxidation products simulated. The atoms in blue, red and green represent choline, phosphate and glycerol groups, respectively. The palmitoyl (*sn*-1) and oleoyl (*sn*-2) chains are represented by black and purple colors, respectively. (b) Two-component heterogeneous membrane composed of POPC molecules (represented in blue) and POPCOOH molecules (represented in green). (For interpretation of the references to colour in this figure legend, the reader is referred to the web version of this article.)

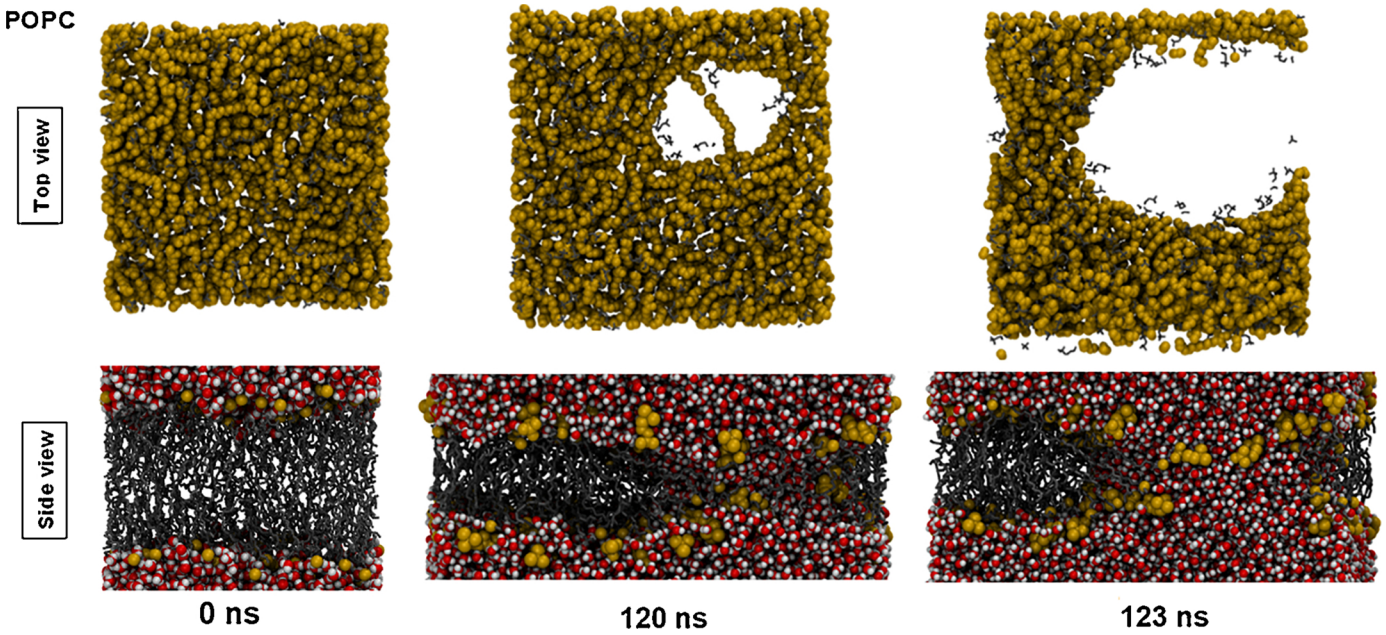


**Fig. 2.** Snapshots from membrane stretching of POPC in 2D at 0.025 nm/ns, starting from the equilibrated membrane. Water molecules and headgroups are represented as van der Waals spheres with red/white and yellow colors, respectively. The *sn*-1 and *sn*-2 chains are represented by gray lines. (For interpretation of the references to colour in this figure legend, the reader is referred to the web version of this article.)

Fig. 1 shows POPC and three of its stable oxidation products at neutral pH used in this study: alcohol (POPCOH), hydroperoxide (POPCOOH) and ketone (POPCO). The oxidation was considered at the C9 with *R*-stereocenter. We studied single-component homogeneous membranes as well as two-component heterogeneous membranes with lipid domains. In the case of homogeneous membranes, each model membrane was entirely composed of POPC or one of its oxidation products in its pure state, with 128 lipid molecules (64 lipid molecules per leaflet) with 46 water molecules per lipid. The initial structure of the heterogeneous membrane was assembled with pre-formed coexisting domains. There was one domain composed of pure POPC (128 lipid molecules) and the other domain was composed of pure POPCOOH (128 lipid molecules). Water was modeled with the *simple point charge* (SPC) model [45]. A Cartesian coordinate system was used with the membrane surface placed parallel to the *xy*-plane and the membrane normal aligned with the *z*-axis. The box used for simulations was

**Table 1**
Summary of simulation conditions and results.

| Entry[a] | Membrane | Simulation conditions[b] | | | | | Replicates | Results[c] | |
|---|---|---|---|---|---|---|---|---|---|
| | | nr. lipids | area ($nm^2$) | COM groups | $v$ (nm/ns) | direction | | $t$ (ns) | $\varepsilon_A$ |
| **1** | **POPC** | 128 | 40 | b/w | 0.025 | *xy* | 2 | 120 / 120 | 1.17(2) |
| **2** | **POPCO** | 128 | 39 | b/w | 0.025 | *xy* | 2 | 96 / 123 | 1.1(1) |
| **3** | **POPCOH** | 128 | 46 | b/w | 0.025 | *xy* | 2 | 93 / 112 | 0.9(1) |
| **4** | **POPCOOH** | 128 | 46 | b/w | 0.025 | *xy* | 2 | 100 / 107 | 0.9(1) |
| **5** | **POPC** | 128 | 40 | b/w | 0.3 | *xy* | 2 | 10 / 12 | 1.3(1) |
| **6** | **POPCO** | 128 | 39 | b/w | 0.3 | *xy* | 2 | 11 / 13 | 1.4(2) |
| **7** | **POPCOH** | 128 | 46 | b/w | 0.3 | *xy* | 2 | 8 / 11 | 1.0(3) |
| **8** | **POPCOOH** | 128 | 46 | b/w | 0.3 | *xy* | 2 | 10 / 11 | 1.1(3) |
| **9** | **POPC** | 128 | 40 | b/w | 0.025 | *x* | 3 | 271 / 280 / 283 | 1.10(1) |
| **10** | **POPCOOH** | 128 | 46 | b/w | 0.025 | *x* | 3 | 205 / 205 / 217 | 0.80(1) |
| **11** | **POPCOOH** | 240 | 83 | b/w | 0.025 | *x* | 1 | 313 | 0.61 |
| **12** | **POPC + POPCOOH** | 256 | 83 | b/w | 0.025 | *x* | 1 | 427 | 0.84 |
| **13** | **POPC** | 276 | 85 | b/w | 0.05 | *x* | 1 | 260 | 1.00 |
| **14** | **POPCOOH** | 240 | 83 | b/w | 0.05 | *x* | 1 | 185 | 0.72 |
| **15** | **POPC + POPCOOH** | 256 | 83 | b/w | 0.05 | *x* | 2 | 194 / 245 | 0.9(1) |
| **16** | **POPC + POPCOOH** | 256 | 85 | d/d/w | 0.025 | *x* | 3 | 320 / 367 / 373 | 0.7(1) |

[a] For clarity, each system is identified by an entry number.
[b] Total number of lipids, initial area, groups for center-of-mass (COM) removal ("b/w" stands for "bilayer and water"; "d/d/w" stands for "native domain, oxidized domain and water"), stretching speed ($v$) and stretching direction ($xy$ for 2D stretching and $x$ for 1D stretching).
[c] Time for pore formation ($t$) for each individual replicate and averaged critical areal strain ($\varepsilon_A$). Uncertainties in the last digit are indicated within parentheses.

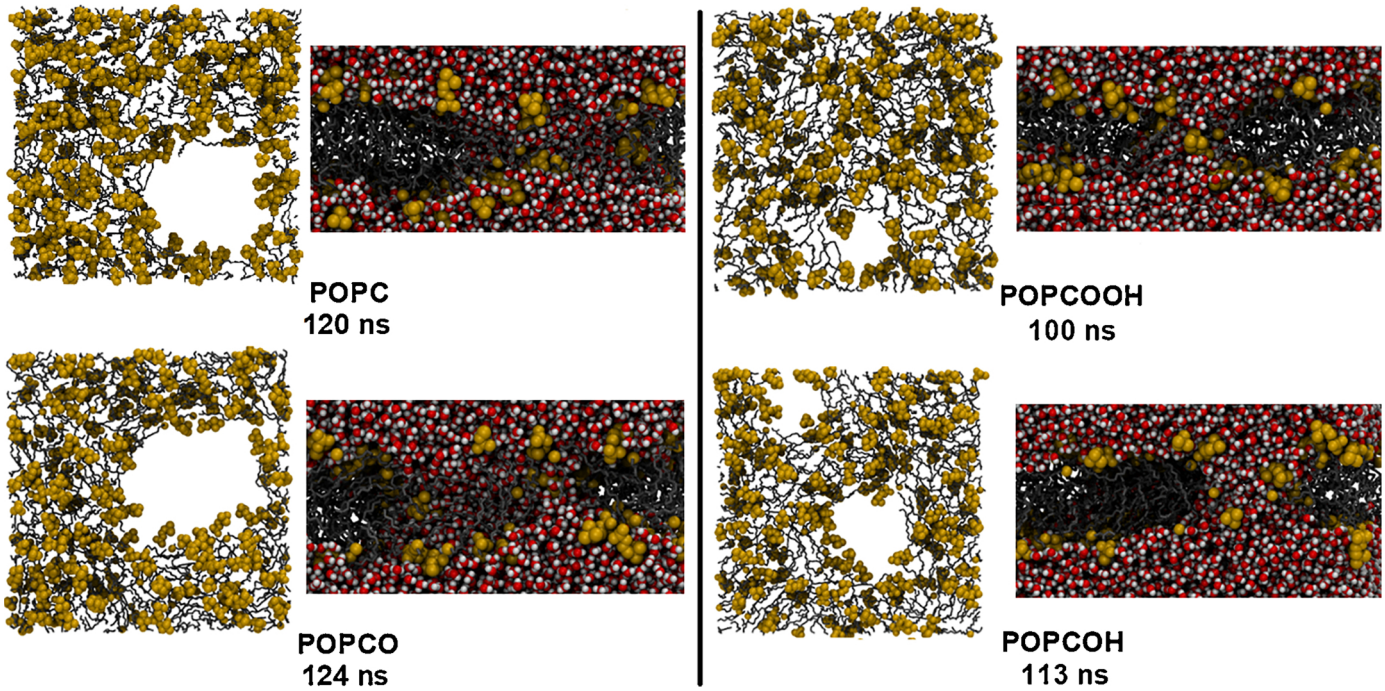


**Fig. 3.** Snapshots from membrane stretching of POPC and its oxidation products in 2D at 0.025 nm/ns.

a cubic box with periodic boundary conditions in three dimensions ($x$, $y$, and $z$).

### 2.2. Simulation details

All simulations were carried out using the software *Groningen machine for chemical simulations* (GROMACS) version 5.0.4 [46] and the united-atom GROMOS 53A6 force field [47] for phospholipid molecules [48]. The parametrization for alcohol and ketone functional groups was taken from the standard GROMOS 53A6 force field library and for hydroperoxide group from well-validated models [6].

We applied the leap-frog algorithm for integrating Newton's equations of motion, using a timestep of 2 fs. For Lennard-Jones interactions, a cut-off radius of 1.4 nm was used. Coulomb interactions were treated using the *particle mesh Ewald* (PME) [49] based on the Ewald summation method. The covalent bond lengths were constrained using the LINCS algorithm [50]. A steepest descent energy minimization was performed prior to equilibration.

Equilibration was performed according to the isothermal-isobaric ensemble (NPT). The temperature was maintained close to the physiological temperature (310*K*) by weakly coupling the system to an external temperature bath using a Nose-Hoover thermostat [51,52]. The temperature coupling relaxation time constant was 0.5 ps. The pressure was maintained close to 1 bar by weakly coupling the system to an external pressure bath using a Parrinello-Rahman barostat [53]. The pressure coupling was applied semi-isotropically, i.e., independently for the extension of the simulation box in the direction of the bilayer normal and for the cross-sectional area of the box in the

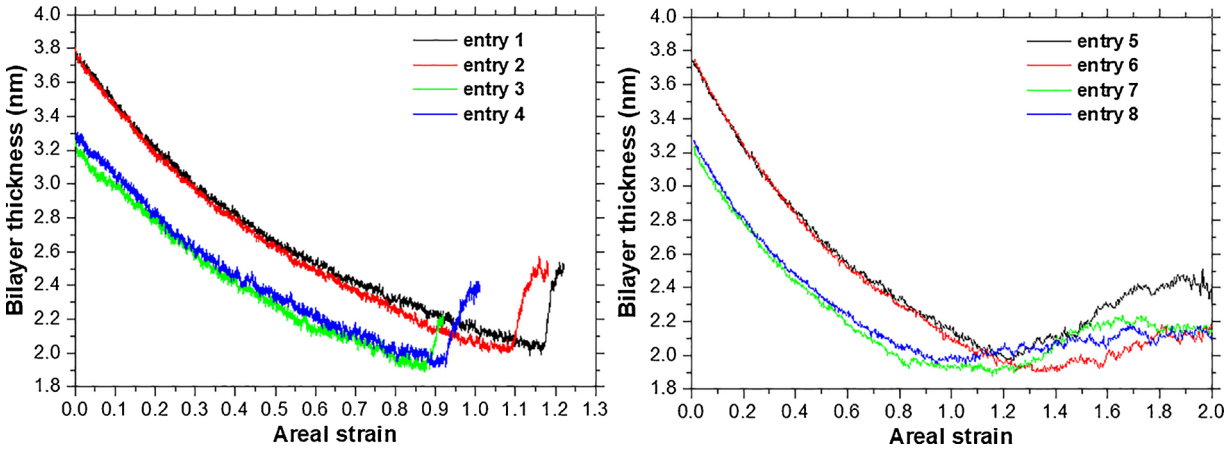


**Fig. 4.** Bilayer thickness versus areal strain ($\varepsilon_A$) for 2D stretching of native and oxidized homogeneous membranes at 0.025 nm/ns (on the left) and at 0.3 nm/ns (on the right). The areal strain was calculated as an average between simulations. Inside the legend, each model membrane is represented by the entries given in Table 1.

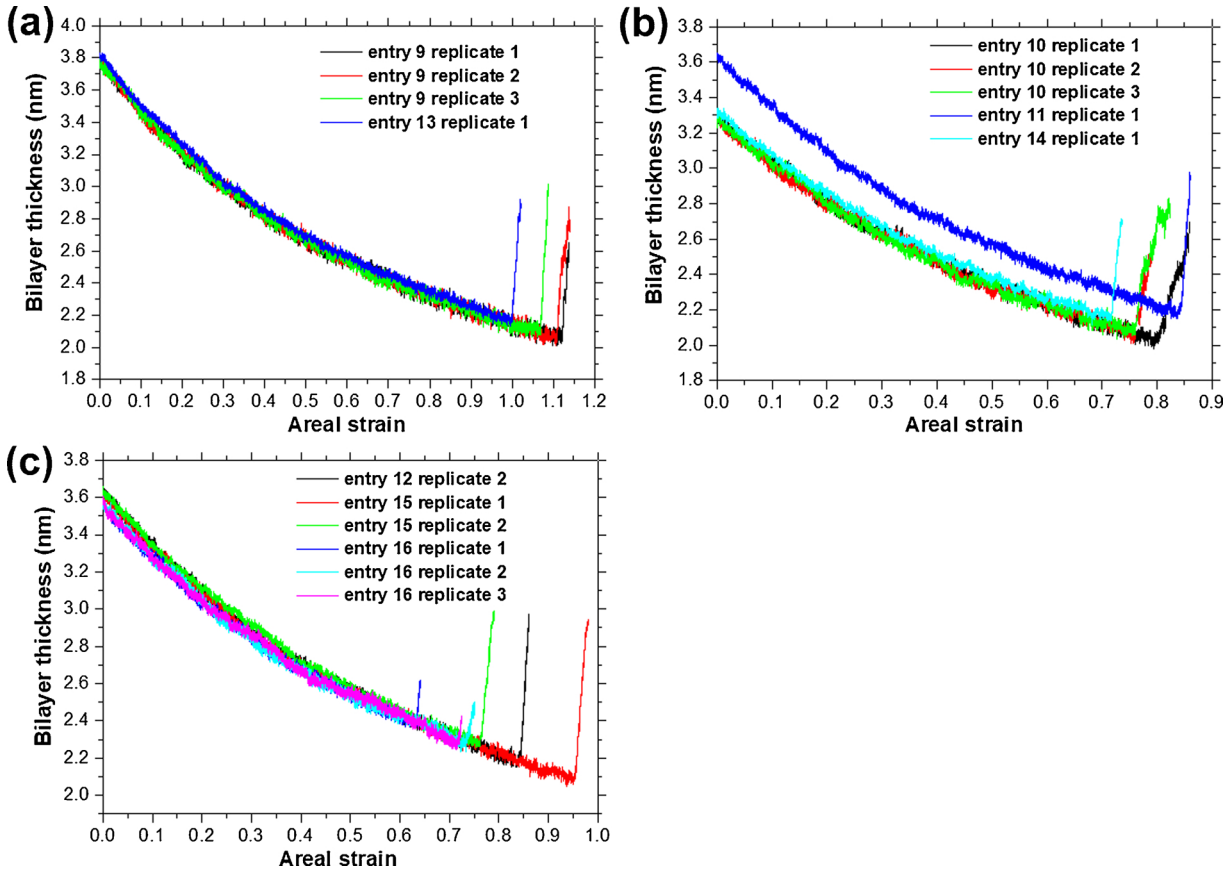


**Fig. 5.** Bilayer thickness versus areal strain ($\varepsilon_A$) for entries 9 and 13 (a), 10, 11 and 14 (b) as well as 12, 15 and 16 (c). Model membranes corresponding to the entries are given in Table 1.

plane parallel to the membrane surface. The pressure coupling relaxation time constant was 2 ps, and the isothermal compressibility of each system was $4.5 \times 10^{-5}$ bar$^{-1}$. We found that an equilibration period of 300 ns was sufficient for convergence of the structural properties such as the membrane area per lipid (see supplementary material). Graphical renderings of the model membranes simulated were produced using the *visual molecular dynamics* (VMD) software [54].

### 2.3. Stretching simulations

After equilibration of the model membranes, we performed non-equilibrium MD simulations of membrane stretching. These simulations involved proportional and temporal scaling of both the atom positions and system box lengths, which is implemented in the GROMACS code as the "deform" option. The model membranes were stretched either in directions *x* and *y* (two dimensions, i.e., 2D), or only in the *x*-direction (one dimension, i.e., 1D). The temperature for lipid and water molecules was individually kept constant at 310 K using the velocity rescaling method [55], with a 0.2 ps coupling time constant. In the model membrane composed of two domains, the system was stretched only in one dimension, namely the direction perpendicular to the domain interface. In the other Cartesian directions, the pressure was kept at 1 bar using an anisotropic Berendsen barostat with a coupling time constant of 0.5 ps and an isothermal compressibility of $4.5 \times 10^{-5}$ bar$^{-1}$.

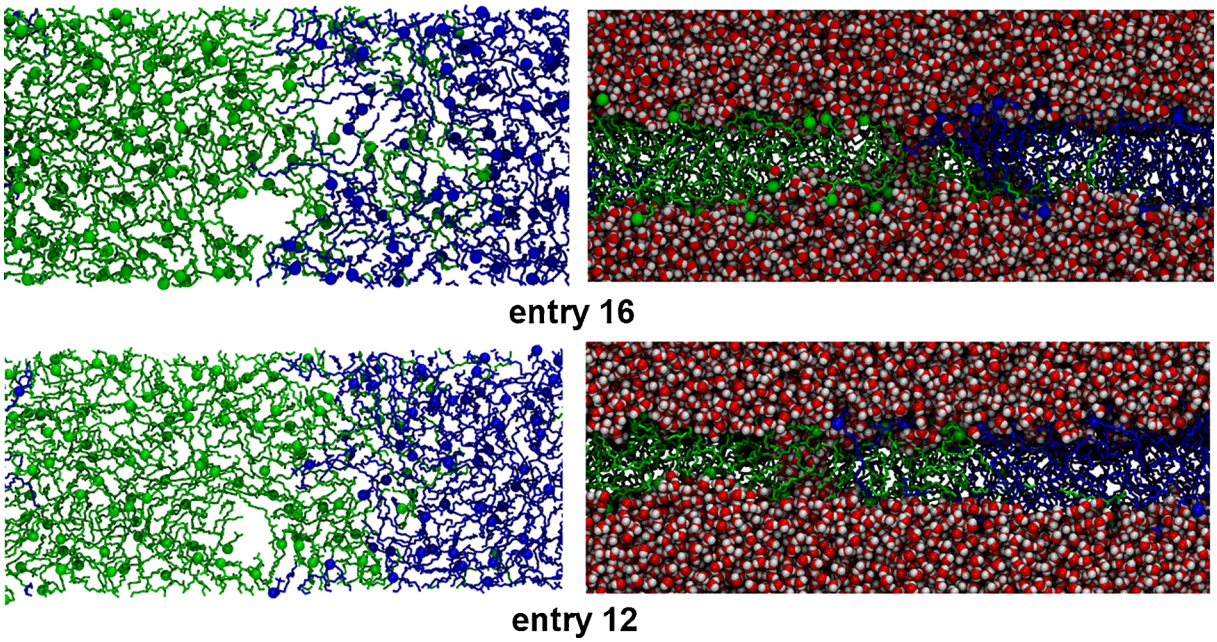


**Fig. 6.** Snapshots of the instant pore formation for entries 16 and 12 (see Table 1). Similar to Fig. 1, POPC and POPCOOH molecules are represented in blue and green colors, respectively. (For interpretation of the references to colour in this figure legend, the reader is referred to the web version of this article.)

Shigematsu and co-workers [56] investigated the effects of stretching speed on mechanical rupture of phosphatidylcholine bilayers using non-equilibrium MD simulations. They investigated stretching speeds varying from 0.025 to 0.3 nm/ns and found that the results at the lowest speeds were reasonably close to the results obtained in experiments at quasi-static stretching. Therefore, we performed our simulations at a speed of 0.025 nm/ns (lower speed). For comparison, data at 0.05 and 0.3 nm/ns (higher speeds) are also presented.

### 2.4. Analysis of membrane properties

The bilayer thickness was obtained by calculating the average position of the upper and lower phosphorus atoms on the *z*-axis, during all simulation time. The area per lipid ($A_L$) was calculated as:

$$A_L = \frac{L_x \times L_y}{n_L}$$

where $L_x$ and $L_y$ are the box size in *x* and *y*-axis, respectively, and $n_L$ the number of lipids in each leaflet.

The first step in the pore formation process is the creation of a narrow water-filled pore across the bilayer [25,41]. We defined the critical areal strain as the value of $\varepsilon_A$ recorded at the very beginning of pore formation, calculated as:

$$\varepsilon_A = \frac{\Delta A}{A_0}$$

where $\Delta A$ is the area variation at a given instant, and $A_0$ is the initial membrane surface area. Because of the statistical nature of pore formation, selected simulations were performed in duplicate or triplicate. The critical $\varepsilon_A$ value was calculated as an average between the simulations.

The instant of pore formation can be identified either by visual inspection of the trajectories or by looking at the time evolution of the membrane thickness. As the membrane is stretched, it becomes ever thinner until a critical $\varepsilon_A$ is reached and a pore is formed. At this moment, the pore grows very rapidly and the membrane thickness increases abruptly due to the release of elastic energy.

## 3. Results and discussion

### 3.1. Molecular mechanism of pore formation in homogeneous membranes

Overall, the process of pore formation is largely driven by structural changes that occurred in each leaflet. Pore formation is accompanied by a reorientation of headgroups towards the bilayer center. As a result, in the pore region a direct interaction between the headgroups located in the opposite leaflets occurs, which leads to the formation of a stable transmembrane pore. After membrane rupture micellization occurs (Fig. 2).

Under lower-speed stretching in 2D, the pore took a longer time to appear due to the lower area expansion rate (Table 1, entries 1–4) and was formed at a larger strain when compared to higher-speed stretching (Table 1, entries 5–8). A possible explanation for that is related to lipid rearrangements. At lower speed, lipids have more time to reorganize themselves, meaning that the membrane is able to resist stretching to a larger degree before the pore finally appears. Under higher speed stretching, the rupture of the membrane occurs quickly after pore formation, because the lipids do not have enough time to rearrange. Besides that, the oxidation reduced the time required for pore formation when compared with native membrane (Fig. 3).

The $\varepsilon_A$ value indicates the relative area variation required for pore formation. When this value exceeds a critical value, water molecules penetrate into the membrane interior and form a pore. The critical $\varepsilon_A$ can be taken as a qualitative indicator of how easy it is, from the energetic point of view, to generate a pore in the membrane. It should be noted, however, that the areal strain depends on the stretching speed. Higher speeds are related to higher values of critical $\varepsilon_A$. As the speed decreases, $\varepsilon_A$ approaches the quasi-static limit. Shigematsu et al. [56] showed that, in the case of phosphatidylcholine membranes, the quasi-static limit can be reasonably approached by a stretching speed as low as 0.025 nm/ns.

The oxidation reduced the critical $\varepsilon_A$ required for pore formation. As the membrane was stretched, the bilayer thickness decreased, and the pore formation was accompanied by reorientation of headgroups inward to the membrane interior. When $\varepsilon_A$ was reached, a pore was formed which soon expanded and caused an abrupt increase in bilayer thickness due to the release of elastic energy. Both under lower and

higher speed (Fig. 4), less strain was required to drive pore formation in POPCOH and POPCOOH, as compared to the native POPC membrane.

Earlier works have suggested that the area compressibility modulus of oxidized membranes is lower than that of native membranes, meaning that oxidized membranes tend to be softer [57]. Therefore, the comparably lower values of critical $\varepsilon_A$ recorded for POPCOH and POPCOOH are also indicative that less energy is required for pore formation in comparison to POPC. Besides that, POPCO presented a critical $\varepsilon_A$ close to POPC, suggesting that this oxidation product alone is not likely to significantly increase membrane permeability.

Recently, we have studied the diffusion of water molecules across oxidative membranes and showed that membrane oxidation reduced the free energy barrier for diffusive water permeation across the membrane [58]. Based on the results reported here, a similar trend is to be expected in the case of pore-mediated permeation. Under mechanical stress, oxidation reduced the critical $\varepsilon_A$. Moreover, POPCOH presented multiple-pores even at lower stretching speed (Fig. 3), demonstrating its susceptibility to water permeation. For POPCOOH and POPCO, multiple pores were observed only under higher speed stretching.

There is large statistical variance in the results. However, we repeated simulations for two selected membranes, namely POPC and POPCOOH, and were able to obtain consistent results under a variety of simulation setup conditions. These include the initial membrane size, stretching speed and direction (Table 1, entries 9–11,13–14). In all cases, oxidized membranes tend to form pores at a smaller areal strain compared to native membranes. Note that larger membranes require longer time for pore formation. To undergo the same relative area variation, larger membranes need to be stretched along a larger distance (i.e. during a longer time period) in comparison to smaller membranes. However, the critical areal strain remains invariant, i.e. it does not depend on the membrane size within statistical uncertainty.

### 3.2. Molecular mechanism of pore formation in heterogeneous membranes

Membrane domains have been shown to form as a consequence of lipid oxidation [34,59], and have been implicated in cellular trafficking and signaling events [60]. In that sense, domain interactions could in principle interfere with transport and signaling events at the cellular level, with possible implications on the pathogenesis of neurodegenerative diseases [61].

Many membrane properties might be largely influenced by the local properties at the interface regions. Recent studies have demonstrated that domain boundaries may be “hot spots” for pore formation and leakage [33]. However, the specific details of how the membrane domains affect membrane permeability have been a matter of discussion.

To investigate this issue, we have assembled a model PLB containing two pre-formed domains: one domain was composed of 100% POPC and the other of 100% POPCOOH. We then performed non-equilibrium MD simulations in which this heterogeneous membrane was stretched in 1D, more specifically in the direction perpendicular to the domain boundaries. Heterogeneous membranes were compared to single-component POPC and POPCOOH membranes with similar size and under similar simulation conditions (Table 1, entries 9–16). We found a large statistical variance of the critical areal strain obtained for the heterogeneous membranes, to the extent that no definitive conclusion could be drawn about the hypothetical influence of the domain interface on the tendency for pore formation. Heterogeneous membranes appeared more prone to pore formation than pure POPC membranes, but they behaved similarly to pure POPCOOH membranes within statistical uncertainty (Fig. 5). Moreover, in heterogeneous membranes, pores formed either at the interface or at the bulk of oxidized domain (Fig. 6). However, results appeared to depend slightly on the algorithm employed for removal of the center-of-mass (COM) motion (Table 1, entries 12, 15–16). We observed that pores tended to form closer to the interface and at a smaller areal strain when the COM motion of individual domains was considered separately. That is probably an artifact that arises from the tension created at the interface region due to the motion of neighboring domains being affected differently by the COM removal algorithm. Further studies, including different and more complex membrane compositions, need to be done to clarify this issue.

The major limitation of our methodology is with respect to size and time scales. We have simulated a system with a pre-formed domain, because phase-separation in lipid membrane occurs on a timescale of tens of microseconds [62]. Thus, it is very difficult to induce membrane domains due to the computational cost. Although we were not inducing domain phase-separation, our results may help to unravel how lipid oxidation affects membrane domains. In the future we would like to investigate whether membrane permeabilization occurs as a consequence of membrane domains and evaluate the possible synergistic effects.

## 4. Conclusions

Taken together, our results showed that membrane oxidation reduced the critical $\varepsilon_A$ and facilitated pore formation under mechanical stress, contributing to membrane leakage. In homogeneous model membranes, the critical areal strain depended on the oxidation product. The oxidation products POPCOH and POPCOOH turned the membrane more susceptible to pore formation, while POPCO had no significant effect. In the case of heterogeneous membranes with coexisting POPC and POPCOOH domains, we could not diagnose whether the interface region was more favorable to pore formation than a bulk POPCOOH phase. Results had a large statistical variance and were dependent on simulation conditions.

## Declaration of Competing Interest

The authors declare that they have no known competing financial interests or personal relationships that could have appeared to influence the work reported in this paper.

## Acknowledgements

We are thankful for the financial support received from the São Paulo Research Foundation (FAPESP) (grant no. 2012/50680-5) and from the National Counsel of Technological and Scientific Development (CNPq) (grant no. 459270/2014-1). MCO acknowledges UFABC for the Master's scholarship granted.

## Appendix A. Supplementary data

Supplementary data to this article can be found online at https://doi.org/10.1016/j.bpc.2019.106266.

## References

[1] G. van Meer, D.R. Voelker, et al., Membrane lipids: where they are and how they behave, Nat. Rev. Mol. Cell Biol. 9 (2008) 112–124.
[2] M.H. Brodnitz, W.W. Nawar, et al., Autoxidation of saturated fatty acids .I. initial products of autoxidation of methyl. palmitate, Lipids 3 (1968) 59–64.
[3] P. Jurkiewicz, A. Olzynska, et al., Biophysics of lipid bilayers containing Oxidatively modified phospholipids: insights from fluorescence and EPR experiments and from MD simulations, Biochim. Biophys. Acta 1818 (2012) 2388–2402.
[4] L. Beranova, L. Cwiklik, et al., Oxidation changes physical properties of phospholipid bilayers: fluorescence spectroscopy and molecular simulations, Langmuir 26 (2010) 6140–6144.
[5] M.A.A. Ayee, E. LeMaster, et al., Molecular-scale biophysical modulation of an endothelial membrane by oxidized phospholipid, Biophys. J. 112 (2017) 325–338.
[6] A.J.P. Neto, R.M. Cordeiro, Molecular simulations of the effects of phospholipid and cholesterol peroxidation on lipid membrane properties, Biochim. Biophys. Acta 1858 (2016) 2191–2198.
[7] L. Cwiklik, P. Jungwirth, Massive oxidation of phospholipid membranes leads to pore creation and bilayer disintegration, Chem. Phys. Lett. 486 (2010) 99–103.
[8] E.J. Szili, S.-H. Hong, et al., On the effect of serum on the transport of reactive oxygen species across phospholipid membranes, Biointerphases 10 (2015) 029511.

[9] M.U. Hammer, E. Forbrig, et al., Influence of plasma treatment on the structure and function of lipids, Plasma Med. 3 (2013) 97–114.
[10] S. Maheux, G. Frache, et al., Small unilamellar liposomes as a membrane model for cell inactivation by cold atmospheric plasma treatment, J. Phys. D. Appl. Phys. 49 (2016) 344001.
[11] S.-H. Hong, E.J. Szili, et al., Ionized gas (plasma) delivery of reactive oxygen species (ROS) into artificial cells, J. Phys. D. Appl. Phys. 47 (2014) 362001.
[12] S. Ki, J. Park, et al., Artificial vesicles as an animal cell model for the study of biological application of non-thermal plasma, J. Phys. D. Appl. Phys. 49 (2016) 085401.
[13] R. Tero, Y. Suda, et al., Plasma irradiation of artificial cell membrane system at solid–liquid interface, Appl. Phys. Express 7 (2014) 077001.
[14] J. Wong-Ekkabut, Z. Xu, et al., Effect of lipid peroxidation on the properties of lipid bilayers: a molecular dynamics study, Biophys. J. 93 (2007) 4225–4236.
[15] M. Yusupov, K. Wende, et al., Effect of head group and lipid tail oxidation in the cell membrane revealed through integrated simulations and experiments, Sci. Rep. 7 (2017) 5761.
[16] J. Van der Paal, E.C. Neyts, et al., Effect of lipid peroxidation on membrane permeability of cancer and normal cells subjected to oxidative stress, Chem. Sci. 7 (2016) 489–498.
[17] M. Yusupov, J. Van der Paal, et al., Synergistic effect of electric field and lipid oxidation on the permeability of cell membranes, Biochim. Biophys. Acta Gen. Subj. 1861 (2017) 839–847.
[18] E. Robert, T. Darny, et al., New insights on the propagation of pulsed atmospheric plasma streams: from single jet to multi jet arrays, Phys. Plasmas 22 (2015) 122007.
[19] A. Shashurin, M. Shneider, et al., Measurements of streamer head potential and conductivity of streamer column in cold nonequilibrium atmospheric plasmas, Plasma Sources Sci. Technol. 21 (2012) 034006.
[20] A.M. Hirst, F.M. Frame, et al., Low temperature plasmas as emerging cancer therapeutics: the state of play and thoughts for the future, Tumor Biol. 37 (2016) 1–11.
[21] P.T. Vernier, Z.A. Levine, et al., Electroporating fields target oxidatively damaged areas in the cell membrane, PLoS One 4 (2009) (e-7966).
[22] T. Kaneko, S. Sasaki, et al., Improvement of cell membrane permeability using a cell-solution electrode for generating atmospheric-pressure plasma, Biointerphases 10 (2015) 029521.
[23] W.-Y. Tai, Y.-C. Yang, et al., Interplay between structure and fluidity of model lipid membranes under oxidative attack, J. Phys. Chem. B 114 (2010) 15642–15649.
[24] K.A. Runas, S.J. Acharya, et al., Addition of cleaved tail fragments during lipid oxidation stabilizes membrane permeability behavior, Langmuir 32 (2016) 779–786.
[25] P. Boonnoy, V. Jarerattanachat, et al., Bilayer deformation, pores, and Micellation induced by oxidized lipids, J. Phys. Chem. Lett. 6 (2015) 4884–4888.
[26] G. Weber, T. Charitat, et al., Lipid oxidation induces structural changes in biomimetic membranes, Soft Matter 10 (2014) 4241–4247.
[27] H.P. Deigner, A. Hermetter, Oxidized phospholipids: emerging lipid mediators in pathophysiology, Curr. Opin. Lipidol. 19 (2008) 289–294.
[28] J.A. Berliner, N. Leitinger, et al., The role of oxidized phospholipids in atherosclerosis, J. Lipid Res. 50 (2009) S207–S212.
[29] M.A. Bradley-Whitman, M.A. Lovell, Biomarkers of lipid peroxidation in Alzheimer disease (AD): an update, Arch. Toxicol. 89 (2015) 1035–1044.
[30] S.R. Shaikh, M.B. Fessler, et al., Role for phospholipid acyl chains and cholesterol in pulmonary infections and inflammation, J. Leukoc. Biol. 100 (2016) 985–997.
[31] C.K. Haluska, M.S. Baptista, et al., Photo-activated phase separation in giant vesicles made from different lipid mixtures, Biochim. Biophys. Acta 1818 (2012) 666–672.
[32] J. Vecer, P. Vesela, et al., Sphingolipid levels crucially modulate lateral microdomain organization of plasma membrane in living yeast, FEBS Lett. 588 (2014) 443–449.
[33] R.M. Cordeiro, Molecular structure and permeability at the Interface between phase-separated membrane domains, J. Phys. Chem. B 122 (2018) 6954–6965.
[34] T.M. Tsubone, H.C. Junqueira, et al., Contrasting roles of oxidized lipids in modulating membrane microdomains, Biochimica Et Biophysica Acta-Biomembranes 1861 (2019) 660–669.
[35] S. Takamori, M. Holt, et al., Molecular anatomy of a trafficking organelle, Cell 127 (2006) 831–846.
[36] G.W. Feigenson, Phase diagrams and lipid domains in multicomponent lipid bilayer mixtures, Biochimica Et Biophysica Acta-Biomembranes 1788 (2009) 47–52.
[37] C. Eggeling, C. Ringemann, et al., Direct observation of the nanoscale dynamics of membrane lipids in a living cell, Nature 457 (2009) 1159–U121.
[38] L.B. Freund, The stiffness of a biomembrane force probe vesicle, Mathematics and Mechanics of Solids 14 (2009) 148–160.
[39] D. Needham, R.S. Nunn, Elastic-deformation and failure of lipid bilayer-membranes containing cholesterol, Biophys. J. 58 (1990) 997–1009.
[40] D.P. Tieleman, H. Leontiadou, et al., Simulation of pore formation in lipid bilayers by mechanical stress and electric fields, J. Am. Chem. Soc. 125 (2003) 6382–6383.
[41] W.F.D. Bennett, N. Sapay, et al., Atomistic simulations of pore formation and closure in lipid bilayers, Biophys. J. 106 (2014) 210–219.
[42] H. Leontiadou, A.E. Mark, et al., Ion transport across transmembrane pores, Biophys. J. 92 (2007) 4209–4215.
[43] M.C. Owen, W. Kulig, et al., Cholesterol protects the oxidized lipid bilayer from water injury: an all-atom molecular Dynamics study, J. Membr. Biol. 251 (2018) 521–534.
[44] A. Schumann-Gillett, M.L. O'Mara, The effects of oxidised phospholipids and cholesterol on the biophysical properties of POPC bilayers, Biochimica Et Biophysica Acta-Biomembranes 1861 (2019) 210–219.
[45] H.J.C. Berendsen, et al., Interaction Models for Water in Relation to Protein Hydration, in: Intermolecular Forces, B. Pullman, Dordrecht, 1981, pp. 331–342.
[46] D. van der Spoel, E. Lindahl, B. Hess, G. Groenhof, A.E. Mark, H.J.C. Berendsen, GROMACS: fast, flexible, and free, J. Comput. Chem. 26 (2005) 1701–1718.
[47] C. Oostenbrink, A. Villa, et al., A biomolecular force field based on the free enthalpy of hydration and solvation: the GROMOS force-field parameter sets 53A5 and 53A6, J. Comput. Chem. 25 (2004) 1656–1676.
[48] D. Poger, A.E. Mark, On the validation of molecular dynamics simulations of saturated and *cis*-monounsaturated phosphatidylcholine lipid bilayers : a comparison with experiment, J. Chem. Theory Comput. 6 (2010) 325–336.
[49] U. Essman, L. Perera, M.L. Berkowitz, T. Darden, H. Lee, L.G. Pedersen, A smooth particle mesh Ewald method, J. Chem. Phys. 103 (1995) 8577–8592.
[50] B. Hess, H. Bekker, et al., LINCS: a linear constraint solver for molecular simulations, J. Comput. Chem. 18 (1997) 1463–1472.
[51] S.A. Nose, Molecular-Dynamics method for simulations in the Canonical ensemble, Mol. Phys. 52 (1984) 255–268.
[52] W.G. Hoover, W.G. Canonical Dynamics, Equilibrium phase-space distributions, Phys. Rev. A 31 (1985) 1695–1697.
[53] M. Parrinello, A. Rahman, Polymorphic transitions in single-crystals - a new molecular-Dynamics method, J. Appl. Phys. 52 (1981) 7182–7190.
[54] W. Humphrey, A. Dalke, K. Schulten, VMD: visual molecular Dynamics, J. Mol. Graph. 14 (1996) 33–38.
[55] G. Bussi, D. Donadio, M. Parrinello, Canonical sampling through velocity rescaling, J. Chem. Phys. 126 (2007) 014101.
[56] T. Shigematsu, K. Koshiyama, et al., Effects of stretching speed on mechanical rupture of phospholipid/cholesterol bilayers: molecular Dynamics simulation, Sci. Rep. 5 (2015) 1–10.
[57] W. Rawicz, B.A. Smith, et al., Elasticity, strength, and water permeability of bilayers that contain raft microdomain-forming lipids, Biophys. J. 94 (2008) 4725–4736.
[58] I.O.L. Bacellar, M.C. Oliveira, L.S. Dantas, et al., Photosensitized membrane permeabilization requires contact-dependent reactions between photosensitizer and lipids, J. Am. Chem. Soc. 140 (2018) 9606–9615.
[59] S. Kim, J. Lee, et al., Plasma-induced water pore formation in model cell membranes: molecular Dynamics simulation, Bull. Kor. Chem. Soc. 39 (2018) 516–523.
[60] K.G.N. Suzuki, Lipid rafts generate digital-like signal transduction in cell plasma membranes, Biotechnol. J. 7 (2012) 753–761.
[61] R. Brandimarti, G.S. Hill, et al., The lipid raft-dwelling protein US9 can be manipulated to target APP compartmentalization, APP processing, and neurodegenerative disease pathogenesis, Sci. Rep. 7 (2017) 1–13.
[62] F.A. Heberle, G.W. Feigenson, Phase separation in lipid membranes, Cold Spring Harb. Perspect. Biol. 3 (2011) 1–13.